

# Interactive segmentation in aerial images: a new benchmark and an open access web-based tool

Zhe Wang<sup>1</sup>, Shoukun Sun<sup>2</sup>, Xiang Que<sup>1,3,\*</sup>, Xiaogang Ma<sup>1</sup>

1. Department of Computer Science, University of Idaho, Moscow, ID 83844, USA

2. Department of Computer Science, University of Idaho, Idaho Falls, ID 83401, USA

3. College of Computer and Information Sciences, Fujian Agriculture and Forestry University, Fuzhou, 350002, China

\* Corresponding Author

## Abstract:

Deep learning has gradually become powerful in segmenting and classifying aerial images. However, in remote sensing applications, the lack of training datasets and the difficulty of accuracy assessment have always been challenges and gaps for the deep learning based classification. In recent years, interactive semantic segmentation proposed in computer vision has achieved an ideal state of human-computer interaction segmentation. It can both provide expert experience and utilize deep learning for efficient segmentation. However, few papers have discussed its application in remote sensing imagery. This study aims to bridge the gap between interactive segmentation and remote sensing image analysis by conducting a benchmark study on various deep learning-based interactive segmentation models. We assessed the performance of five state-of-the-art interactive segmentation methods (Reviving Iterative Training with Mask Guidance for Interactive Segmentation (RITM), FocalClick, SimpleClick, Iterative Click Loss (ICL), and Segment Anything (SAM)) on two high-resolution aerial imagery datasets. The Cascade-Forward Refinement (CFR) approach, an innovative inference strategy for interactive segmentation, was also introduced to enhance the segmentation results without requiring manual efforts. We evaluated these methods on various land cover types, object sizes, and band combinations in the datasets. SimpleClick model consistently outperformed the other methods in our experiments. Conversely, the well-known SAM performed less effectively than other models for remote sensing images. Building upon these findings, we developed a dedicated online tool called RSISeg for interactive segmentation of remote sensing data. RSISeg incorporates a well-performing interactive model that is finetuned with remote sensing data. Compared to existing interactive segmentation tools, RSISeg offers robust interactivity, modifiability, and adaptability to remote sensing data.

**Keywords:** Interactive segmentation; Deep learning; Remote sensing; Land cover classification; Web-based tool

## 1. Introduction

Remote sensing is essential for earth observation and provides valuable insights into land cover, change detection, and semantic segmentation (Audebert et al., 2016; Buitenwerf et al., 2015; Tewkesbury et al., 2015). With the rapid development of remote sensing techniques, remote sensing data have played irreplaceable roles in urban forestry, agriculture, fisheries, etc. (Dauwalter et al., 2017; Khanal et al., 2017; Li et al., 2019; Ma et al., 2019), as they allow for collecting large amounts of data across broad areas and over long periods (Paul and Masehinas, 1981). With its capability of mapping land cover and land use (LULC) and identifying urban development patterns, remote sensing imagery provides accurate and effective solutions for environmental monitoring, resource management, and urban planning (Cheng et al., 2008; Coseo and Larsen, 2014). Analyzing remote sensing images, nonetheless, poses exceptional challenges due to their high dimensionality, complex spectral features, and spatial variability (Camps-Valls et al., 2007).

Deep learning (DL) has emerged as a powerful approach in remote sensing applications in recent years (Falk et al., 2019; Kussul et al., 2017; Ma et al., 2019). Leveraging its ability to automatically learn hierarchical representations from large-scale datasets, DL has demonstrated remarkable performance in the LULC classification (Cheng et al., 2020; Huang et al., 2020; Kussul et al., 2017). DL-based classification models have surpassed the accuracy and efficiency of conventional methods, enabling a more detailed and accurate understanding of land surface dynamics and changes (Yuan et al., 2020). While DL has gained significant popularity in remote sensing, interactive image segmentation has yet to be explored in the context of remote sensing image analysis.

Interactive segmentation and classification techniques are crucial in extracting significant data from satellite and aerial imagery for remote sensing applications. By incorporating user inputs such as scribbles or bounding boxes, interactive image segmentation accurately delimits areas of interest or objects within the image (Jang and Kim, 2019). The interactive approaches allow users to guide the segmentation process by providing additional input, such as scribbles or bounding boxes, to refine and improve the segmentation results (Zhang et al., 2020). Traditionally, these methods required user interactions to divide images into coherent areas and classify land cover features. Approaches such as seed selection, region growing, and user feedback were utilized to refine the segmentation and improve classification accuracy (Espindola et al., 2006; Ferecatu and Boujemaa, 2007; Hossain and Chen, 2019). Ge et al. (2015) developed an interactive segmentation method for high-resolution remote sensing images. Their approach combined hierarchical graph cut algorithms and geodesic distance measures for accurate and interactive segmentation of RGB-D images (Ge et al., 2015). Traditional models in remote sensing segmentation and classification often require manual feature extraction and selection, which can be time-consuming and may not capture the complex relationships within the data. Additionally, they typically need help with the high dimensionality and vast volumes of remote sensing data, limiting their scalability and effectiveness in handling complex, large-scale environmental and geographical analyses.

With the boom in DL technology, interactive image segmentation has achieved impressive progress in computer vision with a wide range of applications, including object recognition, image editing, and medical imaging (Li et al., 2022; Portenier et al., 2018; Suzuki, 2017). Numerous new approaches and techniques have been proposed to address the challenges and limitations of interactive segmentation methods. Sofiiuk et al. (2020) proposed a feature backpropagating refinement scheme (f-BRS), an interactive segmentation method that optimizes intermediate parameters to reduce computation time while improving accuracy (Sofiiuk et al., 2020). Then, his team further proposed Reviving Iterative Training with Mask Guidance for interactive segmentation (RITM) (Sofiiuk et al., 2022). Chen et al. (2022) developed FocalClick, a model that improves efficiency and performance for existing masks, and introduced the Vision Transformer (ViT) backbone to the architecture (Chen et al., 2022). Later in 2022, Liu et al. (2022) proposed SimpleClick, an interactive image segmentation method that achieves good segmentation results with a simple implementation (Liu et al., 2022). Based on the SimpleClick architecture, Sun et al. (2023) introduced a Cascade-Forward Refinement with the Iterative Click Loss (ICL-CFR) model, which consists of three components that can improve segmentation quality without increasing the number of user interactions (Sun et al., 2023). Kirillov et al. (2023) released the Segment Anything Model (SAM), which can accurately segment any object within an image using a single click. They built the largest segmentation dataset to date (Kirillov et al., 2023). Until early 2024, Samsung research conducted experiments to test the robustness of various interactive segmentation models and found that SimpleClick and ICL-CFR are more robust than other evaluated models (Moskalenko et al., 2024). The DL-based interactive segmentation methods allow users to provide feedback to the algorithm and refine the segmentation outputs, resulting in more accurate and reliable segmentation outcomes. However, the unique characteristics and challenges associated with remote sensing images, such as complex spatial patterns, large-scale coverage, and diverse land cover types, necessitate tailored approaches for interactive segmentation in this domain.

Interactive segmentation in remote sensing images has long been a "high threshold" issue, resulting in little discussion in the literature. Demir et al. (2012) studied active-learning techniques in batch mode for the interactive classification of remote sensing images (Demir et al., 2012). The paper extensively discusses batch selection strategies and how this approach can improve the efficiency and accuracy of interactive classification in remote sensing. The purpose of utilizing batch-mode active learning in remote sensing image classification is to curtail annotation efforts by selecting batches of informative samples for labeling. Santos et al. (2013) proposed a method for the interactive classification of remote sensing images using a multiscale segmentation (dos Santos et al., 2013). This method leveraged boosting-based active learning to select regions based on user feedback at varying scales, leading to better classification results than isolated scales. Demir et al. (2011) introduced a new interactive domain-adaptation technique utilizing active learning to adapt a supervised classifier trained on one remote sensing image to classify a distinct but related target image (Demir et al., 2011). Additionally, Hichri et al. (2012) presented a change detection technique based on interactive segmentation requiring users to enter labels relevant to the changed and unchanged classes in the different images (Hichri et al., 2012). Interactive segmentation in remote sensing faces challenges such as the slow integration of real-time user feedback, variability in human input leading to inconsistent training data, and balancing automation with user control. Strategies to enhance DL models for interactive segmentation include creating lightweight, quickly updated models, employing active learning to incorporate user input efficiently, and using transfer learning to generalize across different datasets with minimal new input. These improvements aim to make DL models more responsive, consistent, and scalable for practical remote sensing applications.

In conclusion, this study aims to bridge the gap between interactive segmentation and remote sensing image analysis by conducting a benchmark study on various deep learning-based interactive segmentation models. In this study, our main contributions are:

- (1) We investigated how well the current state-of-the-art interactive segmentation methods perform on two ISPRS datasets.
- (2) We evaluated interactive segmentation methods on diverse land cover types, object sizes, and band combinations.
- (3) We developed a novel online tool for interactive segmentation focusing on remote-sensing images based on the findings from the experiments and further compared our tool with the SAM model.

## **2. Materials and methods**

### **2.1 Dataset**

In this study, we acquired Potsdam and Vaihingen datasets for model training from ISPRS (Figure 1). Potsdam and Vaihingen datasets are high-resolution aerial imagery datasets designed for semantic labeling and object detection tasks ("Vaihingen 2D Semantic Labeling - ISPRS," n.d.). The Potsdam dataset covers a 42.4-hectare urban area in Potsdam, Germany, and comprises several gigabytes of red (R), green (G), blue (B), and near-infrared (IR) imagery. The images have a spatial resolution of 5 cm per pixel. The Vaihingen dataset covers a 16 km<sup>2</sup> area in Vaihingen, Germany, and consists of high-resolution RGBIR imagery with a spatial resolution of 9 cm. Both datasets include six labeled object classes: roads, buildings, trees, and cars. Computer vision and remote sensing researchers have widely used the datasets to benchmark and evaluate algorithms for semantic segmentation and object detection.

Based on these two datasets, we remade them into four datasets with different band combinations, PRGB (Potsdam RGB), PRGIR (Potsdam RGBIR), PRGBIR (Potsdam RGBIR) and VRGIR (Vaihingen RGBIR).

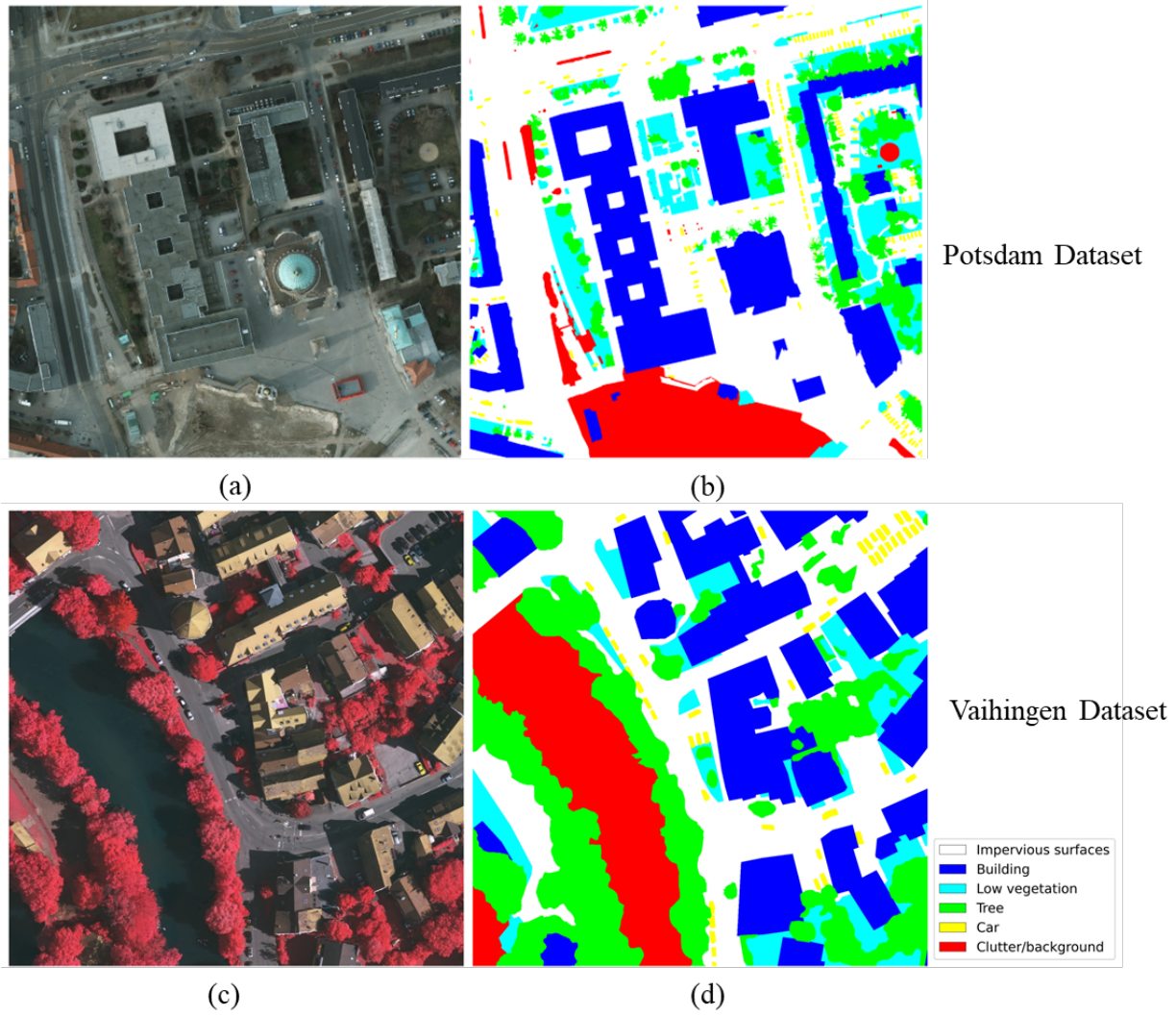


Figure 1. Example patch of Potsdam Dataset (RGB image (a) and corresponding label (b)) and Vaihingen Dataset (RGB image (c) and corresponding label (d)) image

## 2.2 Data preprocessing

We evaluated models by harnessing the potential of all four datasets (PRGB, PRGIR, PRGBIR, and VRGIR). The Potsdam dataset contains 38 images featuring four bands (R, G, B, IR). Of the 38 images, we selected 32 for training, leaving 6 for testing. Every image has a pixel size of  $6000 \times 6000$  and a spatial resolution measure of 5 cm. The Vaihingen dataset has 33 images: 27 for training and 6 for testing. Each Vaihingen image is approximately  $2000 \times 2500$  pixels with 9cm spatial resolution. Both datasets possess six shared common classes.

As these two datasets are semantic segmentation datasets, we revisited them and morphed them into instance segmentation datasets. This was achieved through a process: each image was broken down into patches, and every continuous label belonging to a specific class within a patch was transformed into an object. The Potsdam dataset was broken down into patches of  $600 \times 600$  pixel-size each. The aftermath of this transformation left the training dataset containing 3200 patches and 47152 objects, while the testing dataset featured 600 patches and 10365 objects. Regarding the Vaihingen dataset, after its transformation, we ended up with a training dataset with 1770 patches and 20102 objects and a testing dataset of 385 patches and 4651 objects.



## **2.3 Representable models**

In interactive semantic segmentation, common interaction methods often include point-based, bounding box, freehand, and scribble interaction (Pavoni et al., 2022). Point-based interaction has several practical advantages in interactive segmentation. Point-based interaction in interactive segmentation offers precision and efficiency. The specific localization of points allows users to pinpoint areas of interest accurately, resulting in precise segmentation. It's efficient due to minimal interaction cost, requiring only a few clicks or keypresses. This makes it ideal for users to review and refine segmentation results in a feedback loop, allowing prompt corrections or improvements.

### **2.3.1 Reviving Iterative Training with Mask Guidance for Interactive Segmentation (RITM) (Sofiiuk et al., 2022)**

The RITM uses a feedforward model for click-based segmentation to focus on interactive segmentation without additional optimization schemes. It allows for segmenting new objects and refining existing masks iteratively. The model leverages segmentation masks from previous steps to enhance accuracy and stability, achieving state-of-the-art results without the need for backward passes during inference. The training dataset choice significantly impacts segmentation quality, with a combination of COCO and LVIS datasets (Gupta et al., 2019; Lin et al., 2014) showing superior performance. The proposed method emphasizes simplicity and effectiveness in interactive segmentation tasks.

### **2.3.2 FocalClick (Chen et al., 2022)**

FocalClick addresses the challenges of interactive image segmentation by introducing an efficient pipeline that decomposes the heavy inference task into two lighter predictions on smaller patches. Unlike some earlier models, which might rely strictly on traditional Convolutional Neural Networks (CNNs) or don't utilize the previous masks for iterative refinement, FocalClick incorporates both CNN and ViT architectures. This dual-architecture approach allows FocalClick to leverage the spatial hierarchies captured by CNNs and the global context understanding facilitated by ViTs, providing more nuanced and accurate segmentation outputs. FocalClick also distinguishes itself by utilizing previous masks as part of its input for refinement, suggesting an iterative, feedback-driven approach to improving segmentation accuracy. This feature allows the system to progressively refine the segmentation output based on user inputs, making the tool more interactive and user-friendly, especially in complex segmentation tasks where precision is crucial.

### **2.3.3 SimpleClick (Liu et al., 2022)**

SimpleClick introduces a novel approach to interactive image segmentation by leveraging only a plain ViT backbone. The model utilizes a masked autoencoder (MAE) pretraining strategy to capture meaningful representations efficiently. By adapting the ViT backbone for interactive segmentation with minimal modifications, SimpleClick achieves state-of-the-art performance in segmentation tasks. The deep neural network architecture divides input images into fixed-size patches, which are linearly projected into vectors and processed through a series of Transformer blocks for self-attention. This streamlined approach allows SimpleClick to extract objects accurately with limited user interaction, making it a practical and efficient tool for semantic segmentation tasks across various domains.

### **2.3.4 ICL-CFR (Sun et al., 2023)**

Based on SimpleClick, the CFR-based inference strategy for semantic segmentation iteratively refines segmentation results without requiring two separate models. This method employs a deep neural network for segmentation, where the network generates coarse segmentation masks through incremental user interactions (outer loop) and refines these masks by forwarding the segmentation model multiple times with the same input image and user clicks (inner loop). The model inputs include raw images, maps generated by clicks, and previous segmentation masks. The CFR strategy is defined by equations that

describe how the model iteratively updates the segmentation masks based on the input image, user clicks, and the previous mask, aiming for higher segmentation quality with fewer clicks.

### 2.3.5 SAM (Kirillov et al., 2023)

The SAM developed by Meta is an advanced segmentation model capable of accurately segmenting any object within an image using just a single click. SAM is a promotable segmentation system that can generalize its segmentation capabilities to unfamiliar objects and images without additional training. SAM's exceptional performance is attributed to its extensive training on a large dataset of 11 million images and 1.1 billion masks. This comprehensive training allows SAM to generate masks for all objects in an image effectively. Alternatively, users can provide specific points or guidance to SAM, enabling the model to generate precise masks tailored to a particular object of interest. Table 1 outlines the evolution and capabilities of five interactive segmentation models evaluated in this study.

Table 1. Comparison between different models

Models	Input			Refinement	Backbone		Year
	Image	Clicks	Previous Mask		CNN	ViT	
<b>RITM</b>	✓	✓	×	×	✓	×	2021
<b>FocalClick</b>	✓	✓	✓	✓	✓	✓	2022
<b>SimpleClick</b>	✓	✓	✓	×	×	✓	2022
<b>ICL-CFR</b>	✓	✓	✓	✓	×	✓	2023
<b>SAM</b>	✓	✓	✓	×	×	✓	2023

### 3. Experiments and results

Our experiments were conducted in three steps to evaluate the performance of various interactive segmentation models, comprising five models, as mentioned in section 2.3. For pre-trained models, we conducted experiments using the initial weights. We trained finetuned models using the hyperparameters provided by the authors in the original article. We improved RITM and SimpleClick models using Sun's proposed CFR method. The CFR is not applied with FocalClick because it has a local refinement module. In the first step, we evaluated eight models: SimpleClick, SimpleClick-CFR, ICL, ICL-CFR, RITM, RITM-CFR, FocalClick, and SAM. Following this, we finetuned and tested the models on remote sensing datasets, Potsdam and Vaihingen, to assess their performance. In the initial step, the SAM and FocalClick models demonstrated poor performance compared to the other models. Thus, we compared ICL, RITM, SimpleClick, and their CFR versions in the second step. However, all discussed models initially required three-channel input, while the Potsdam dataset images contain four bands. Hence, in the third step, we examined the performance of various interactive segmentation methods with various band combinations and land cover types, including plot sizes under different land cover types. Finally, we found that the SimpleClick model to be the best performer, and we modified its input structure to test its performance on four-band remote sensing data, inputting all four bands from the PRGBIR dataset. Table 2 provides the experiment summary for each model.

Table 2. Experiments of each model on different datasets

Model Name	Pretrained	PRGB	PRGIR	VRGIR	PRGBIR
SimpleClick	✓	✓	✓	✓	✓
SimpleClick-CFR	✓	✓	✓	✓	✓
ICL	✓	✓	✓	✓	×
ICL-CFR	✓	✓	✓	✓	×

RITM	✓	✓	✓	✓	×
RITM-CFR	✓	✓	✓	✓	×
FocalClick	✓	×	×	×	×
SAM	✓	×	×	×	×

### 3.1 Evaluation of models using initial weights

We evaluated the model performance using the number of clicks (NoC) (Sofiuk et al., 2020) and the average click number required to reach the target intersection over the union (IoU) (Nowozin, 2014). It measures how many clicks or interactions a user provides to achieve a desired result. Lower NoC suggests a more efficient model as it requires fewer user interactions for accurate segmentation. The average click number needed to reach the target IoU can be found using iterative interaction and segmentation mechanisms. Initially, the model might generate an initial segmentation with low IoU. Then in the subsequent iterations, additional user clicks can be introduced to improve the segmentation until the target IoU is reached. We reported the NoC to achieve the IoU at four levels of evaluation, 80%, 85%, 90%, and 95%, which correspond to the metrics NoC80, NoC85, NoC90, and NoC95, respectively.

Figure 3 illustrates example patches featuring RGB imaging, RGIR imaging, and individual imaging across four separate bands (R, G, B, IR) within the VRGBIR dataset. A RGIR composite image in remote sensing can help make the vegetation appear clearer and more differentiated from other features. This is because it utilizes the near-infrared band, a spectrum to which vegetation strongly responds. Chlorophyll in healthy vegetation absorbs visible light (0.4 - 0.7  $\mu\text{m}$ ) for use in photosynthesis, whereas the cell structure of the leaves strongly reflects near-infrared light (0.7 - 1.1  $\mu\text{m}$ ) (Uchegbulam and Ayolabi, 2013). Hence, vegetation typically appears bright red when viewed in an RGIR composite image (where infrared data is often coded in red), making it easier to identify and examine.

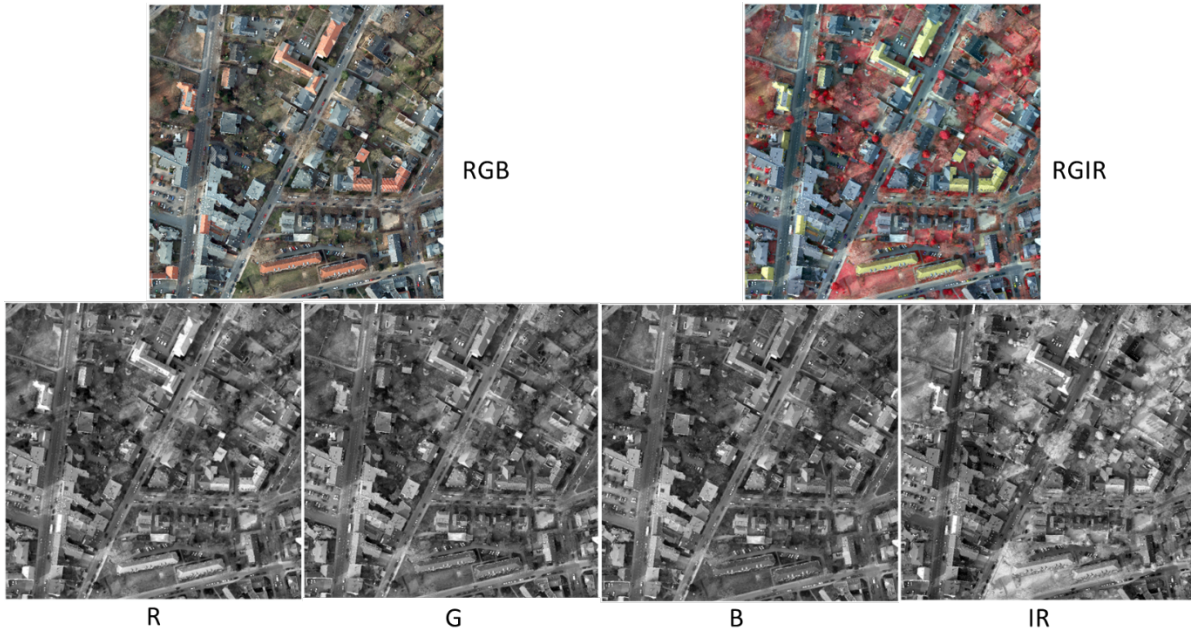


Figure 3. Comparative visualization of RGB, RGIR, R, G, B, and IR imaging

Table 3 shows the performance of different interactive segmentation models on PRGB and PRGIR datasets without finetuning at varying IoU levels. On the PRGB dataset, RITM demonstrates the best performance at the 80% IoU level. The SimpleClick-CFR model performs best at the higher IoU levels

(85%, 90%, and 95%), demonstrating its ability to achieve finer and more accurate segmentation results. Except for SAM and Focal Click, the remaining models exhibit similar performance at the higher IoU levels (85%, 90%, and 95%). However, as the desired IoU level increases, the efficiency of all models declines significantly. While the least-performing model at the 80% IoU level requires less than seven clicks, at the 95% IoU level, even the best-performing model, SimpleClick-CFR, requires approximately fourteen clicks. This trade-off between precision and efficiency becomes evident at higher IoU thresholds. On the PRGIR dataset, SimpleClick and SimpleClick-CFR consistently demonstrate strong performance across multiple IoU thresholds. SimpleClick requires the fewest clicks at 80% IoU and maintains its superiority at 85%, 90%, and 95% IoU levels. RITM and RITM-CFR models also exhibit competitive performance across different IoU thresholds. However, SAM consistently requires the highest number of clicks, indicating comparatively lower performance.

Table 3. Evaluation results on PRGB and PRGIR datasets without finetuning

Model Name	PRGB				PRGIR			
	NoC80	NoC85	NoC90	NoC95	NoC80	NoC85	NoC90	NoC95
SimpleClick	4.90	6.27	8.84	14.31	<b>4.83</b>	6.45	<b>9.24</b>	14.95
SimpleClick-CFR	4.94	<b>6.26</b>	<b>8.80</b>	<b>14.28</b>	4.90	<b>6.44</b>	9.29	<b>14.83</b>
ICL	5.04	6.47	9.10	14.61	5.10	6.65	9.64	15.24
ICL-CFR	5.14	6.54	9.15	14.62	5.11	6.73	9.63	15.20
RITM	<b>4.78</b>	6.34	9.22	14.89	5.22	6.87	10.00	15.52
RITM-CFR	4.81	6.34	9.23	14.90	5.36	7.08	10.14	15.53
FocalClick	5.56	7.05	9.70	15.01	5.26	6.96	10.04	15.28
SAM	6.58	8.77	12.34	17.54	6.78	9.34	13.36	17.78

Figure 4 reveals the varying trends of mIoU for eight distinct models as the number of clicks increases from 1 to 10. The RITM-CFR model is the most effective at the outset with a single click. As the click count rises from 2 to 4, the performance of the SAM model remains consistent and comparable to both RITM and RITM-CFR. Yet, once the click count surpasses 5, SAM persistently registers a slight underperformance relative to the other models. Upon reaching 10 clicks, all models display a mIoU near 0.9, except SAM, which falls below 0.85.

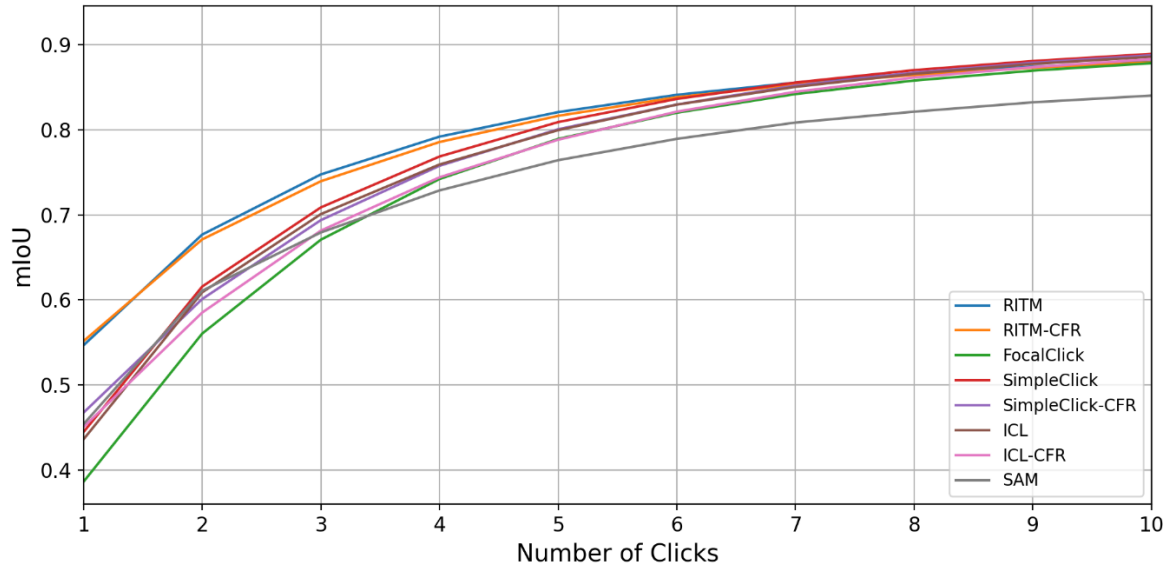


Figure 4. Mean IoU (mIoU) given  $n$  clicks ( $n$  ranges from 1 to 10) of eight models.

### 3.2 Models evaluations after finetuning

Table 4 shows the results of interactive segmentation models after finetuning. SimpleClick and SimpleClick-CFR consistently exhibit superior performance with lower click counts across all IoU thresholds, indicating their remarkable efficiency in user interaction for accurate segmentation. The "ICL" and "ICL-CFR" models exhibit slightly higher click counts, indicating an increased level of user interaction. However, they still deliver reasonable performance with a moderate number of clicks to achieve accurate segmentation results. Similarly, the "RITM" and "RITM-CFR" models present slightly higher click counts but maintain efficient user interaction to achieve accurate segmentations.

Table 4. Evaluation results on PRGB and PRGIR datasets after finetuning

Model Name	PRGB				PRGIR			
	NoC80	NoC85	NoC90	NoC95	NoC80	NoC85	NoC90	NoC95
SimpleClick	3.26	4.39	6.73	12.47	3.30	4.42	6.77	12.45
SimpleClick-CFR	3.28	4.39	6.74	12.45	3.27	4.39	6.77	12.43
ICL	3.70	5.04	7.69	13.61	4.32	5.87	8.90	15.01
ICL-CFR	3.64	4.95	7.59	13.55	4.16	5.73	8.74	14.93
RITM	3.92	5.36	8.18	14.10	4.18	5.67	8.60	14.45
RITM-CFR	3.86	5.30	8.13	14.03	4.16	5.62	8.54	14.36

Figure 5 provides a comparative analysis of the mIoU for models, both finetuned and non-finetuned, as the number of clicks varies from 1 to 10. With only one click, finetuned models already achieve a mIoU exceeding 0.6. As the click count progressively increases, the finetuned models consistently outperform their non-finetuned counterparts. However, the performance gap, as quantified by the mIoU, between the two types of models steadily narrows. By the point where the number of click counts hits 10, the superior performance of the finetuned models, though still discernible, approximates that of the non-finetuned models, with scores hovering around 0.9.

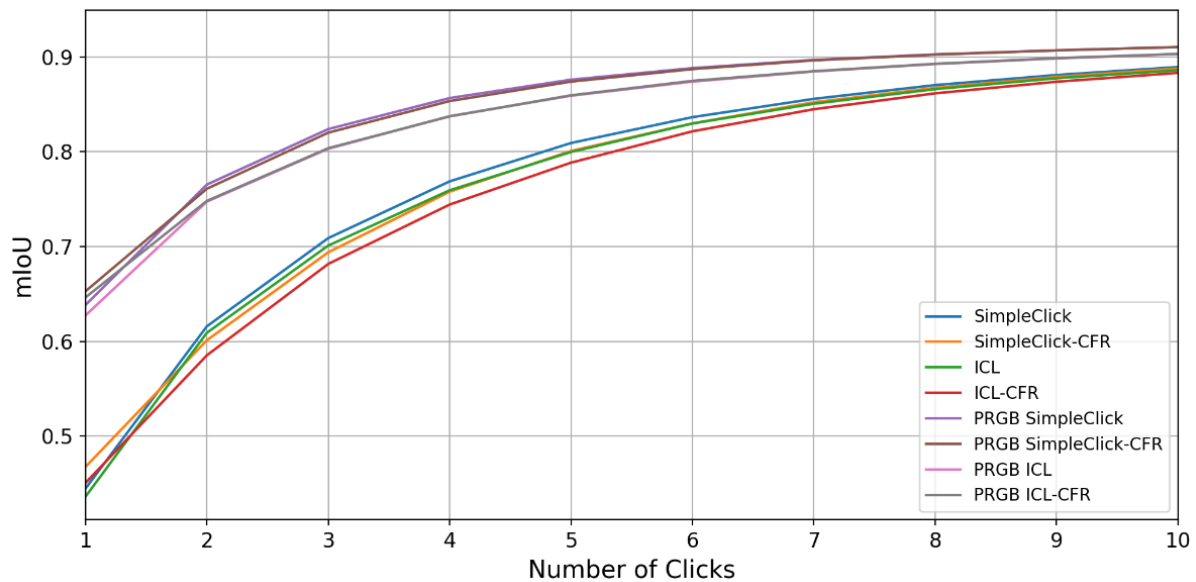


Figure 5. Comparison of mean IoU (mIoU) given  $n$  clicks ( $n$  ranges from 1 to 10) between models before and after finetuning.

Table 5 demonstrates the evaluation results on the VRGIR dataset before and after finetuning with the PRGIR dataset. Among the various models we evaluated, the SimpleClick models consistently outperformed the others, achieving superior results across all IoU levels while requiring fewer user clicks

for interactive segmentation. These findings highlight the robustness and efficiency of the SimpleClick model in the context of multispectral data. Moreover, comparing all the models to the baseline model that was not finetuned and directly evaluated on the VRGIR dataset, we observed significant improvements in performance across the board. These results underscore the importance of finetuning models on relevant datasets to enhance their performance on specific tasks, such as interactive segmentation using multispectral imagery.

Table 5. Evaluation results on VRGIR dataset before and after finetuning

Model Name	Before finetuning				After finetuning			
	NoC80	NoC85	NoC90	NoC95	NoC80	NoC85	NoC90	NoC95
SimpleClick	4.16	5.70	8.43	<b>14.19</b>	<b>4.83</b>	6.45	<b>9.24</b>	14.95
SimpleClick-CFR	<b>4.16</b>	<b>5.67</b>	<b>8.34</b>	14.22	4.90	<b>6.44</b>	9.29	<b>14.83</b>
ICL	5.24	6.95	10.16	15.72	5.10	6.65	9.64	15.24
ICL-CFR	5.17	6.92	10.21	15.73	5.11	6.73	9.63	15.20
RITM	4.81	6.60	9.65	15.19	5.22	6.87	10.00	15.52
RITM-CFR	4.84	6.47	9.62	15.15	5.36	7.08	10.14	15.53

Figure 6 demonstrates the substantial improvement in model performance when the finetuned models are applied to the VRGIR dataset. Notably, the SimpleClick-CFR model demonstrates the highest level of improvement, exhibiting a remarkable increase of 33.15% at the 80% IoU level. However, it is worth noting that the models show less improvement at the 95% IoU level, suggesting that reaching higher levels of accuracy becomes progressively challenging.

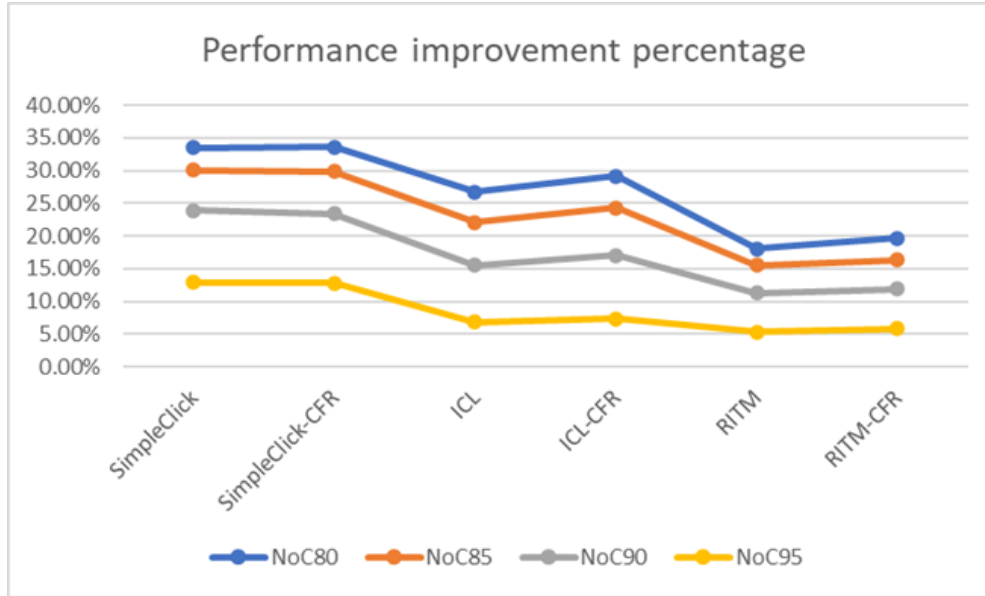


Figure 6. Performance improvement percentage between the modes before and after finetuning.

### 3.3 Model performance by different classes

Tables 6 and 7 present the results of various interactive segmentation models on several classes: ‘Impervious Surface’, ‘Building’, ‘Low Vegetation’, ‘Tree’, and ‘Car’, respectively. Given that all models exhibit a similar trend in their results, this paper focuses solely on the evaluation performance of the PRGB dataset after finetuning.

After finetuning, Table 6 presents the evaluation results on different land cover types of various interactive segmentation models on the PRGB dataset. In the SimpleClick model, we observed differing levels of performance across classes. The "Building" class achieved the lowest number of clicks required for accurate segmentation, indicating the model's ability to segment buildings with minimal user input. Conversely, the 'Low Vegetation' class presented a more significant challenge, with more clicks required for satisfactory results. The "Tree" class required an intermediate number of clicks, while the 'Car' class required more clicks for successful segmentation. Similar trends were also observed in the SimpleClick-CFR model, with the "Building" class demonstrating the lowest number of clicks (1.83) required for an 80% IoU. For the 'Low Vegetation' class, 4.17 clicks were necessary, while the 'Tree' class needed 3.27 clicks, and the "Car" class required 1.79 clicks for similar IoU levels.

Table 6. Evaluation results by class on the PRGB dataset

<b>Class</b>	<b>Impervious surface</b>	<b>Building</b>	<b>Low vegetation</b>	<b>Tree</b>	<b>Car</b>
<b>Model Name</b>	<b>Noc80/95</b>	<b>Noc80/95</b>	<b>Noc80/95</b>	<b>Noc80/95</b>	<b>Noc80/95</b>
SimpleClick	3.53/12.33	<b>1.85/4.63</b>	4.11/13.49	3.22/12.45	1.76/10.45
SimpleClick-CFR	3.55/12.28	<b>1.83/4.69</b>	4.17/13.47	3.27/12.36	1.79/10.46
ICL	4.07/13.67	1.96/5.10	4.77/14.70	3.62/14.16	1.99/11.67
ICL-CFR	3.97/13.62	1.99/5.04	4.70/14.64	3.57/14.07	1.98/11.58
RITM	4.46/14.62	2.30/6.14	4.89/15.22	4.11/14.55	2.09/11.95
RITM-CFR	4.42/14.48	2.31/6.20	4.82/15.07	4.01/14.58	2.01/11.86

Table 7 shows the performance of different interactive segmentation models after finetuning the PRGB dataset. Notably, the observed trend in this table aligns with the patterns observed in Table 4, indicating consistency in the model performances across the evaluated datasets. One intriguing observation is that despite the expected benefits of utilizing the IR band for vegetation segmentation, such as trees and grass, Table 5 reveals a lower efficiency in most classes. This finding suggests that the inclusion of the IR band in the segmentation process may only sometimes lead to improved results, highlighting the complexity and variability of the segmentation task across different land cover classes.

Moreover, consistent with the observations made in Table 1, it is evident that achieving higher IoU levels, particularly at 95%, requires a significantly higher number of clicks. The findings demonstrate that except for the car class, which exhibits a more minor increase, all other classes require approximately three times more clicks to reach the desired IoU level from 80% to 95%. Notably, the car class stands out, necessitating around nine times more clicks, as exemplified by the SimpleClick model, where the click counts increase from 1.85 to 10.40.

Table 7. Evaluation results by different land cover types on the PRGIR dataset

<b>Class</b>	<b>Impervious surface</b>	<b>Building</b>	<b>Low vegetation</b>	<b>Tree</b>	<b>Car</b>
<b>Model Name</b>	<b>Noc80/95</b>	<b>Noc80/95</b>	<b>Noc80/95</b>	<b>Noc80/95</b>	<b>Noc80/95</b>
SimpleClick	<b>3.55/12.25</b>	1.79/4.68	<b>4.17/13.51</b>	3.14/12.30	1.85/10.40
SimpleClick-CFR	3.55/12.24	<b>1.78/4.67</b>	4.18/13.42	<b>3.12/12.27</b>	<b>1.83/10.48</b>
ICL	4.72/15.10	2.29/6.09	5.56/15.78	4.01/15.56	2.36/14.54
ICL-CFR	4.56/15.11	2.23/5.89	5.40/15.63	3.86/15.55	2.29/14.41
RITM	4.62/15.00	2.51/6.58	5.33/15.47	4.47/15.13	2.19/12.38
RITM-CFR	4.68/14.92	2.52/6.63	5.30/15.38	4.49/15.09	2.16/12.20

### 3.4 Model performance on different segment sizes



In remote sensing land cover classification, the size of surface objects is a crucial factor (Weng, 2012). We further investigated the relationship between the size of surface objects and the number of clicks required to achieve various IoU thresholds in interactive segmentation. This analysis aimed to gain insights into the impact of object size on the interactive segmentation process and explore any potential variations in the number of required clicks across different land cover classes at different IoU levels. For our experiments on interactive segmentation, we considered five land cover types, among which the shapes of buildings and trees exhibit relative regularity and variations compared to the other classes. Tables 8 and 9 present the performance of different interactive segmentation models specifically for buildings and trees of varying sizes.

In Table 8, the segment size of the building class was divided into five categories ranging from  $0.075 \text{ m}^2$  to  $881.90 \text{ m}^2$  using the quantile method. Figure 8 shows an example of the different building sizes in the images. It is noticeable that larger building segments require fewer clicks to achieve satisfactory IoU levels across the interactive segmentation models. This indicates that the segmentation algorithms are more efficient in dealing with larger building segments than smaller ones. Interestingly, when comparing the building class's performance with other land cover classes, we observed that buildings require fewer clicks for successful segmentation. This is attributed to their regular and well-defined shape characteristics, which facilitate the interactive segmentation process, resulting in reduced click requirements for different segment sizes.

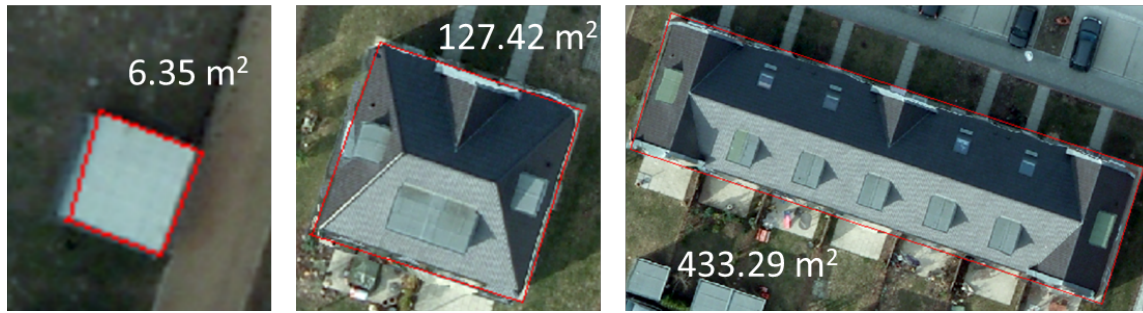


Figure 7. Examples of different sizes of the building segments

Table 8. Building class evaluation results at various segment Sizes on PRGB dataset

Size Model Name	( $0.075 \text{ m}^2$ , $9.03 \text{ m}^2$ ] <sup>a</sup>	( $9.03 \text{ m}^2$ , $36.36 \text{ m}^2$ ]	( $36.36 \text{ m}^2$ , $100.08 \text{ m}^2$ ]	( $100.08 \text{ m}^2$ , $256.83 \text{ m}^2$ ]	( $256.83 \text{ m}^2$ , $881.90 \text{ m}^2$ ]
	Noc80/95	Noc80/95	Noc80/95	Noc80/95	Noc80/95
SimpleClick	<b>3.76/12.11</b>	1.483.78	<b>1.36/2.92</b>	1.36/2.25	<b>1.28/2.06</b>
SimpleClick-CFR	3.62/12.36	<b>1.47/3.87</b>	1.37/2.88	<b>1.38/2.28</b>	1.30/2.03
ICL	3.91/12.48	1.63/4.53	1.41/3.38	1.38/2.65	1.44/2.42
ICL-CFR	3.99/12.37	1.63/4.54	1.41/3.27	1.43/2.56	1.48/2.44
RITM	4.09/13.99	1.60/4.76	1.50/3.93	1.68/3.29	2.64/4.72
RITM-CFR	3.83/13.78	1.62/4.76	1.53/4.20	1.80/3.41	2.76/4.81

a. The notation ( $0.075 \text{ m}^2$ ,  $9.03 \text{ m}^2$ ] indicates an interval that includes all segment sizes greater than  $0.075 \text{ m}^2$  up to and including  $9.03 \text{ m}^2$ . The parenthesis '('' signifies that the number immediately following it is not included in the interval, while the bracket '['' signifies that the number immediately before it is included.

Table 9 outlines the segment sizes of the tree class, dividing them into five categories using the quantile method, ranging from  $0.075 \text{ m}^2$  to  $847.53 \text{ m}^2$ . An intriguing observation is that smaller land objects require more clicks to achieve accurate segmentation, a pattern consistent across all evaluated models.

This indicates a consistent relationship between object size and the complexity of the segmentation task. Remarkably, the optimal performance in terms of click efficiency is observed within a specific range of sizes, with the best results obtained for land objects ranging from 155.93 m<sup>2</sup> to 847.53 m<sup>2</sup>. This suggests that interactive segmentation models achieve a favorable balance between accuracy and the number of required clicks within this size range, resulting in more efficient and reliable segmentation outcomes.

Table 9. Tree class evaluation results at various segment sizes on the PRGB Dataset

Model Name \ Size	(0.075 m <sup>2</sup> , 1.96 m <sup>2</sup> ] <sup>a</sup>	(1.96 m <sup>2</sup> , 9.52 m <sup>2</sup> ]	(9.52 m <sup>2</sup> , 37.12 m <sup>2</sup> ]	(37.12 m <sup>2</sup> , 155.93 m <sup>2</sup> ]	(155.93 m <sup>2</sup> , 847.53 m <sup>2</sup> ]
	Noc80/95	Noc80/95	Noc80/95	Noc80/95	Noc80/95
SimpleClick	<b>3.55/12.25</b>	1.79/4.68	<b>4.17/13.51</b>	3.14/12.30	1.85/10.40
SimpleClick-CFR	3.55/12.24	<b>1.78/4.67</b>	4.18/13.42	<b>3.12/12.27</b>	<b>1.83/10.48</b>
ICL	4.72/15.10	2.29/6.09	5.56/15.78	4.01/15.56	2.36/14.54
ICL-CFR	4.56/15.11	2.23/5.89	5.40/15.63	3.86/15.55	2.29/14.41
RITM	4.62/15.00	2.51/6.58	5.33/15.47	4.47/15.13	2.19/12.38
RITM-CFR	4.68/14.92	2.52/6.63	5.30/15.38	4.49/15.09	2.16/12.20

a. The notation (0.075 m<sup>2</sup>, 1.96 m<sup>2</sup>] indicates an interval that includes all segment sizes greater than 0.075 m<sup>2</sup> up to and including 1.96 m<sup>2</sup>. The parenthesis '('' signifies that the number immediately following it is not included in the interval, while the bracket '['' signifies that the number immediately before it is included.

### 3.5 Performance evaluation with 4-Band dataset (PRGBIR)

Table 10 displays the models' performance on the PRGBIR dataset, which consists of four bands, offering more spectral information than the three-band input. Nevertheless, the results in Table 8 demonstrate that the models trained on the PRGBIR dataset have worse segmentation accuracy and overall performance than those trained on three-band input, as shown in Tables 4 and 5. These findings suggest that despite the inclusion of the additional band, its incorporation does not lead to improved performance. Therefore, it is crucial to carefully consider the impact of different spectral bands and their relevance to the specific task. Increasing the number of input channels does not necessarily translate into improved performance.

Table 10. Evaluation results on PRGBIR dataset

Class \ Model	SimpleClick	SimpleClick-CFR
	Noc80/85/90/95	Noc80/85/90/95
Impervious Surface	3.96/5.06/7.50/13.40	3.88/4.98/7.43/13.37
Building	2.00/2.37/3.06/5.02	1.93/2.27/2.93/4.91
Low Vegetation	4.65/6.11/8.80/14.13	4.60/5.95/8.65/14.02
Tree	3.75/4.83/7.09/13.06	3.76/4.82/6.98/13.05
Car	2.03/2.64/4.15/11.18	1.95/2.50/3.83/10.88
Overall	3.72/4.97/7.46/13.11	3.65/4.83/7.30/13.02

## 4. Interactive segmentation tool for remote sensing data, RSISeg tool

Drawing on the findings from the above experiments, we developed an online tool, RSISeg, for interactive segmentation, specifically tailored to remote sensing imagery. This tool integrates models finetuned with remote sensing data from our earlier experiments and incorporates the original SAM model. To optimize its functionality for remote sensing data, the tool is engineered to process TIFF files

efficiently and export results in GeoJSON format. This capability simplifies the re-editing process across various GIS software platforms.

Figure 8 depicts the interactive segmentation process in the tool used to delineate land cover objects. The figure demonstrates the use of two types of points: positive clicks and negative clicks. Positive clicks are placed directly on the target land cover segment, indicating the desired area for inclusion. Conversely, negative clicks are positioned on regions considered irrelevant or not belonging to the intended segment, serving as markers for exclusion. To maintain the balance between efficiency and accuracy in line with our experimental findings, it is advisable to exercise caution and stay within 20 clicks for a single land cover segment. Going beyond this limit could decrease the quality and efficiency of segmentation. Therefore, users should exercise caution and provide a reasonable number of clicks within this limit. By adhering to this guideline, users can optimize the interactive segmentation process and balance accuracy and the time required for segment delineation.

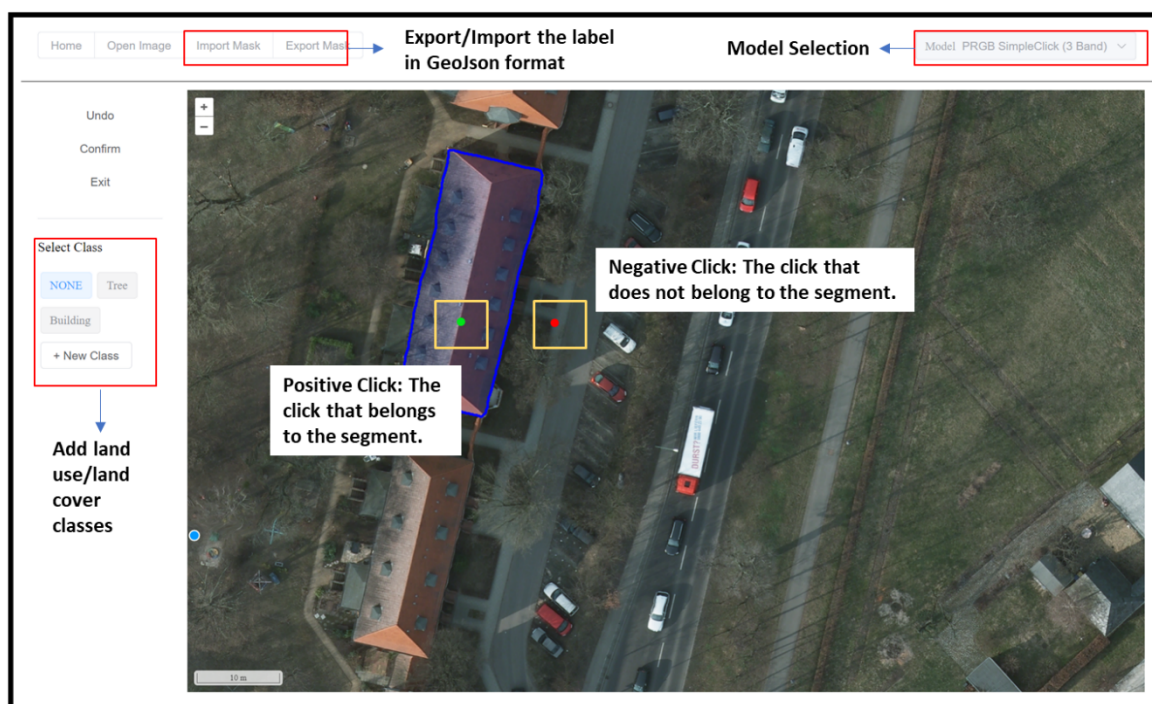


Figure 8. RSISeg user interface screenshot

Figure 9 portrays the product derived from the interactive segmentation process. The generated segmented land cover objects can be exported in a GeoJSON format, thus facilitating additional analyses and integration with geospatial software, such as QGIS (“Welcome to the QGIS project!,” n.d.). The tool has two pre-established classes: 'Tree' and 'Building', allowing users to append more classifications. As demonstrated in Figure 9, the 'Car' class was added. Moreover, the tool assigns distinct colors to the

different land object classes.

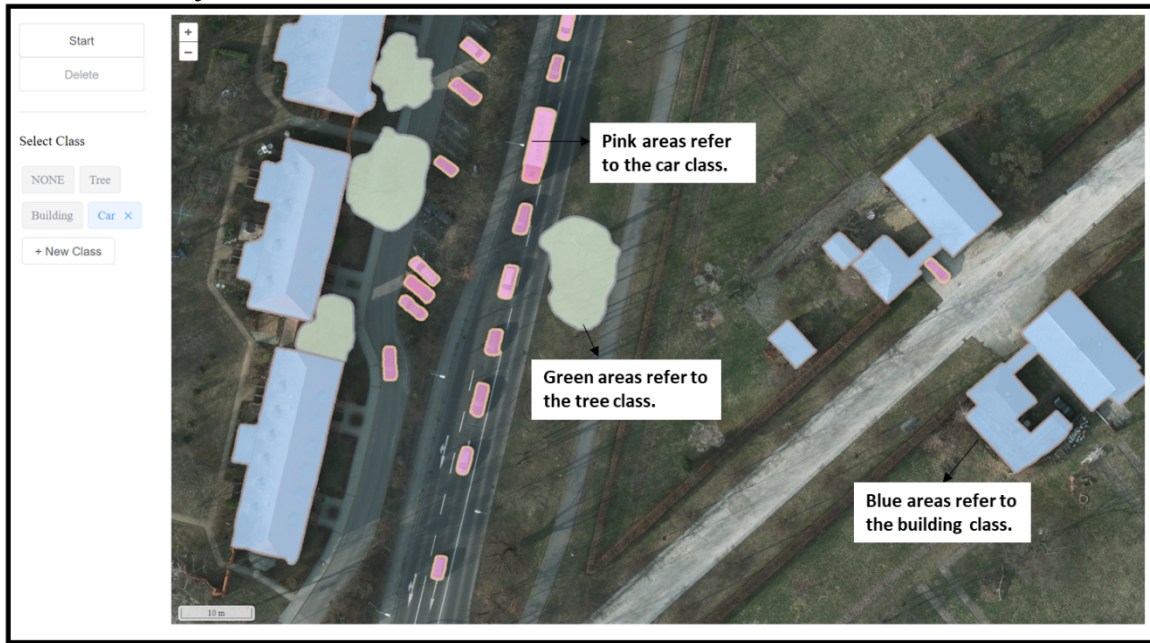


Figure 9. Example interactive segment results

## 5. Discussion

Interactive segmentation marks a significant advancement in the application of remote sensing technologies, particularly in enhancing the accuracy and utility of classified imagery data. Deep learning techniques have improved remote sensing in the era of rapid technological evolution. Yet, the necessity of achieving high precision in image classification has brought about challenges. Despite its prowess in handling massive datasets and automating the classification process, deep learning often requires labor-intensive validation or fieldwork, which questions its efficiency and accuracy.

In response to these challenges, interactive segmentation emerges as a solution that synergizes human expertise with machine efficiency. Unlike traditional methods that rely solely on automated algorithms, interactive segmentation incorporates human judgment into the classification process. This method requires minimal human input, such as drawing boundaries or marking areas of interest in an image, which the algorithm then uses to refine its understanding and improve segmentation results. This blend of human intuition and machine processing ensures more accurate outcomes, as it allows for the nuanced detection of patterns and features that automated systems might overlook. Moreover, incorporating interactive segmentation into remote sensing applications has far-reaching implications. It facilitates the creation of high-precision datasets for deep learning semantic segmentation and directly contributes to producing land cover classification products with unprecedented accuracy. This enhanced precision is crucial for various applications, including environmental monitoring, urban planning, agriculture, and climate change research, where the accuracy of segmented remote sensing images can significantly impact decision-making and policy development.

Our analysis of different interactive segmentation models has provided valuable insights into their performance and applicability in remote sensing. One notable observation is that the SimpleClick models, namely SimpleClick and SimpleClick-CFR, have consistently exhibited the best performance across various evaluation metrics. These models have displayed their remarkable generalization ability for remote sensing images, surpassing the ICL model's performance reported in previous studies on different

datasets. This highlights the efficacy and versatility of the SimpleClick models in the context of interactive segmentation tasks within the remote sensing domain.

One crucial aspect we explored was the impact of different band combinations on the models' performance. Including the NIR band proved significant for vegetation monitoring and analysis. The NIR band captures essential information related to vegetation health, density, and other relevant parameters. Therefore, we conducted experiments using different band combinations, including RGB and RGIR, expecting models trained on the PRGIR dataset to excel in segmenting trees and grass. However, the results displayed in Table 9 and Table 10 indicate that the performance of the models on both PRGB and PRGIR datasets remains comparable, suggesting that the models can effectively handle vegetation segmentation regardless of the specific band combination. In addition to vegetation, we focused on other land cover classes, such as buildings, impervious surfaces, and cars. Among these classes, buildings demonstrated the most favorable results, as their regular and well-defined shapes facilitated accurate segmentation. The models consistently performed well in segmenting buildings, indicating their ability to effectively capture this class's distinct characteristics.

Furthermore, we extended our analysis to explore the relationship between the size of land cover objects and the models' segmentation performance. Interestingly, we observed that smaller land objects required more clicks for accurate segmentation. This finding suggests that smaller objects' fine details and intricate structures necessitate additional user input for precise delineation. Combining these findings, we can conclude that the discussed models exhibit promising performance in remote sensing applications. They highlight the ability to effectively segment various land cover classes, including vegetation and buildings, while highlighting the influence of object size on the segmentation process.

However, SAM, which has been trained on an extensive dataset containing many images and masks, surprisingly displayed the poorest performance among the models evaluated in our study. Despite its large-scale training data, SAM's performance did not match the expectations set by the SimpleClick models. This discrepancy may suggest that the complexity and unique characteristics of remote sensing images require a tailored approach that considers specific domain knowledge and considerations. In greater depth, we have compared SAM and the best model in this study, SimpleClick. Figure 10 illustrates the process: when segmenting a building, the segmentation results of SAM and SimpleClick with one positive point at the exact location, two positive points, respectively, and the number of points required by the two models to achieve the final segmentation target. Upon administering a single click, SimpleClick segments an entire building anchored on the clicked location, while SAM only segments half of the building, delineated by the building's ridge. A second click placed on the building's opposite side results in SimpleClick and SAM sketching out the full building; however, the edges marked by SAM are noticeably more jagged. By adding negative points to isolate unwanted areas, SimpleClick attains a satisfying segmentation result with just one negative point, equating to three clicks. Conversely, SAM only manages to meet user satisfaction after incorporating several additional points, and the edges of its segmented objects continue to display roughness.



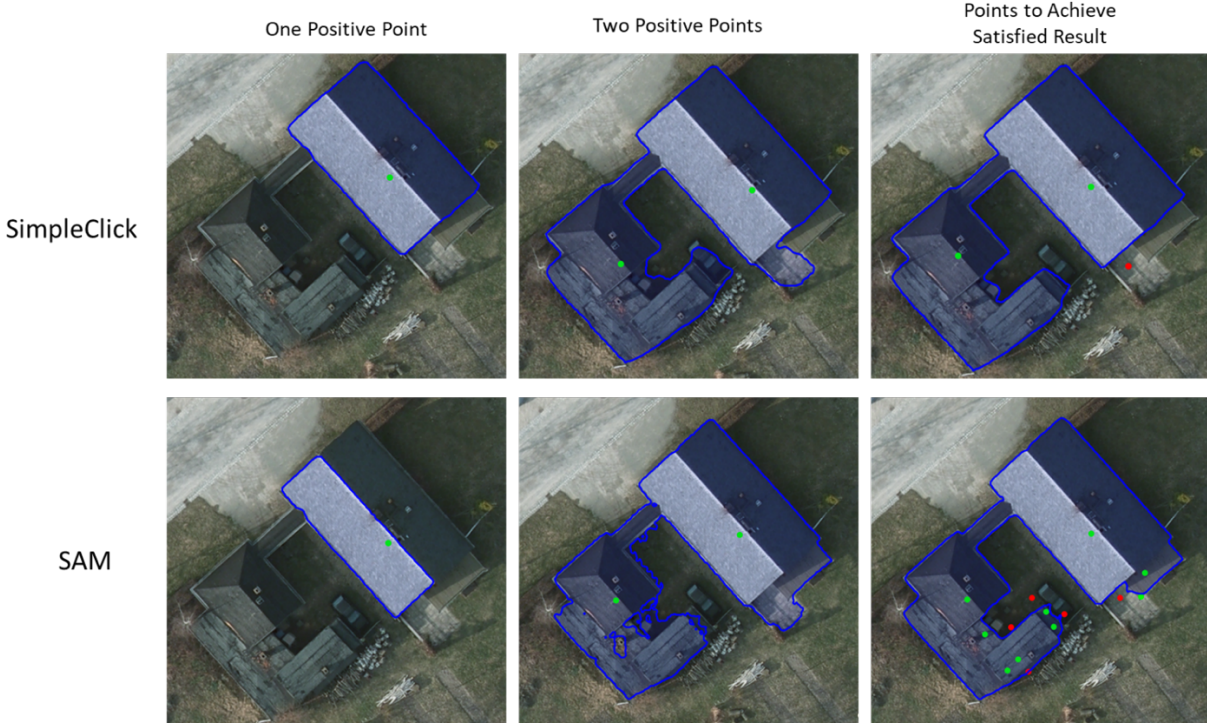


Figure 10. Comparison between SimpleClick and SAM through the visualized processes of building segmentation.

Figure 11 displays the percentage of total segments achieving various IoU results for SimpleClick, SimpleClick-CFR, and SAM models when the click count totals 2 and 5. In Figure 11(a), with a click count of 2, all segments with an IoU between 0-0.6 constitute less than 5% of the total. Meanwhile, for segments with an IoU greater than 0.8, both SimpleClick-CFR and SAM models register a larger count than SimpleClick. Moving to Figure 11(b), when the number of clicks increases to 5, the SAM model exhibits the highest segment proportion at an IoU, around 0.7. However, when the segments hit an IoU of 0.95, both SimpleClick and SimpleClick-CFR markedly surpass SAM.

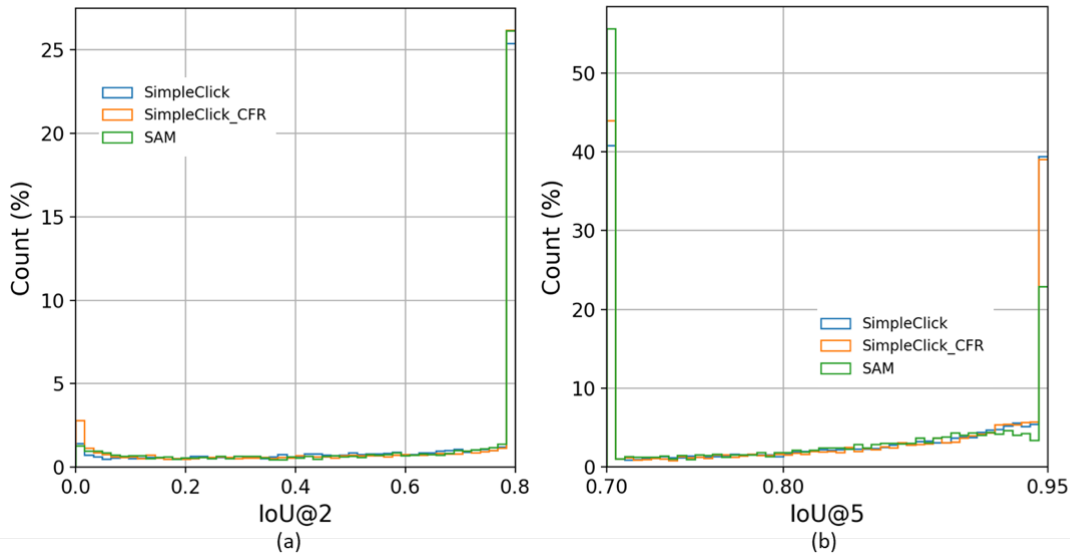


Figure 11. Histogram analysis for the segmentation results given  $k = 2$  and 5.

In the SAM paper, the authors compare SAM with RITM, FocalClick, and SimpleClick, which are mentioned in this article (Kirillov et al., 2023). SAM can achieve lower single-point performance, consistent with the conclusion drawn from Figure 11(a). This indicates that when the number of clicks is limited, especially in the range of 1-5, SAM can more readily yield a positive result (with an IoU exceeding 70%). However, for more refined segmentation requirements, SimpleClick/SimpleClick-CFR can more readily help the IoU to attain over 90% with more input. Given the diverse shapes of landmark objects in urban land classification, Figure 10 also hints that SAM might not excel in outlining the edges of landmark objects. This could be why the classification results of SimpleClick/SimpleClick-CFR models are superior.

The demo tool provided by SAM supports several different prompts, including 'point,' 'box,' 'mask,' and 'arbitrary format text.' However, we only compared SAM's 'point' prompt mode in this study. While SAM's model is powerful for automatic segmentation tasks, this paper discusses click-based interactive segmentation models. SAM has been widely discussed recently. Therefore, our tool has also integrated the primarily click-based SAM model. Some proposed geo-based SAM tools, such as the SAM tool of ArcGIS Pro ("Introduction to the model—ArcGIS pretrained models | Documentation," n.d.) and SAMJS, developed by AntV. However, most of them lack interactivity and efficiency.

Therefore, we further developed a high-interactivity tool, RSISeg, designed to perform interactive segmentation on remote sensing data. This tool presents notable attributes, as delineated below:

1. RSISeg is explicitly engineered to facilitate the handling of remote sensing data. It is endowed with an ability to read TIFF (Tagged Image File Format) data and export GeoJSON files complete with coordinates, enabling swift editing within GIS (Geographic Information Systems) software. Remote sensing imagery, often characterized by more than three spectral bands and differing satellite data types, can be seamlessly imported to the tool, and relevant parameters edited accordingly.
2. The tool offers superior interactivity compared to other interactive segmentation tools. It flourishes with features such as data window scaling, positive point-negative point addition, and retroactive deleting alterations, enriching user-software interactions significantly.
3. Furthermore, RSISeg is adept at categorizing land use and land cover in remote sensing imagery. We have pre-defined two common types associated with remote sensing classifications: 'Tree' and 'Building.' Users have the liberty to add classifications as per their requirements. This tool garnishes different classifications with diverse color schemes in the results for easier deciphering. We have incorporated several models in this tool that have been proven effective in discerning remote sensing data through empirical evidence and finetuning. These models include SimpleClick, SimpleClick-CFR, ICL, ICL-CFR, and SAM.

The tool is open-access and available via <http://tickmap.nkn.uidaho.edu/rsis/>. Moving forward, it is envisaged that this tool will be optimized further, augmenting it, making it capable of executing automated segmentation and accumulative learning and delivering enhanced classification of land use based on remote sensing imagery.

## 6. Conclusion

This paper evaluates the robustness and efficiency of the latest interactive segmentation models in remote sensing. Various remote sensing datasets and an in-depth analysis of different band combinations, object sizes, and object categories were tested. Segmentation can be directly achieved with only about two points for larger and simpler objects, such as buildings over 160 square meters. Meanwhile, through testing different models and comparing them with the currently popular SAM model, we have identified SimpleClick as the most efficient and robust model. Based on all conclusions, we have developed an online interactive segmentation tool for remote sensing images utilizing a fine-tuned model. This tool



considers the uniqueness of remote sensing image data. The output results can also be edited further using various GIS software. This achievement represents a significant advancement in remote sensing image processing, offering a practical solution that enhances the accessibility and applicability of interactive segmentation for professionals in the field.

In the future, based on the research and conclusions of this paper, many improvements can be made. We can utilize the developed tool to create more training samples, enhancing the model's accuracy in classifying remote sensing images. Furthermore, there is room for improvement in the model, particularly the ICL-CFR model, regarding remote sensing data. Remote sensing images and objects are more complex compared to conventional pictures. The CFR process can be repeated to enable the model to learn more from previously obtained results. Additionally, the refinement process could be modified to fully use the information from previous masks. In summary, the uniqueness of remote sensing images allows for detailed analysis in both interactive segmentation and deep learning aspects.

### **Funding**

This work is supported by the National Science Foundation under Grant No. 2019609, the National Natural Science Foundation of China (42202333), and the Natural Science Foundation of Fujian Province (2021J05030 and 2022J01152).

### **CRedit authorship contribution statement**

Z.Wang: Conceptualization, Data curation, Formal analysis, Investigation, Methodology, Visualization, Writing – original draft, Writing – review & editing. S.Sun: Formal analysis, Visualization, Methodology – review & editing. X.Que: Funding acquisition, Supervision, Validation, Writing-review & editing. X.Ma: Funding acquisition, Writing – review & editing.

### **Declaring of competing interest**

The authors declare that they have no known competing financial interests or personal relationships that could have appeared to influence the work reported in this paper.

### **Reference:**

- Audebert, N., Saux, B.L., Lefèvre, S., 2016. Semantic Segmentation of Earth Observation Data Using Multimodal and Multi-scale Deep Networks. arXiv:1609.06846 [cs].
- Buitenwerf, R., Rose, L., Higgins, S.I., 2015. Three decades of multi-dimensional change in global leaf phenology. *Nature Climate Change* 5, 364.
- Camps-Valls, G., Marsheva, T.V.B., Zhou, D., 2007. Semi-supervised graph-based hyperspectral image classification. *IEEE transactions on Geoscience and Remote Sensing* 45, 3044–3054.
- Chen, X., Zhao, Z., Zhang, Y., Duan, M., Qi, D., Zhao, H., 2022. FocalClick: Towards Practical Interactive Image Segmentation, in: *Proceedings of the IEEE/CVF Conference on Computer Vision and Pattern Recognition*. pp. 1300–1309.
- Cheng, G., Xie, X., Han, J., Guo, L., Xia, G.-S., 2020. Remote sensing image scene classification meets deep learning: Challenges, methods, benchmarks, and opportunities. *IEEE Journal of Selected Topics in Applied Earth Observations and Remote Sensing* 13, 3735–3756.
- Cheng, K.-S., Su, Y.-F., Kuo, F.-T., Hung, W.-C., Chiang, J.-L., 2008. Assessing the effect of landcover changes on air temperature using remote sensing images—A pilot study in northern Taiwan. *Landscape and Urban Planning* 85, 85–96.
- Coseo, P., Larsen, L., 2014. How factors of land use/land cover, building configuration, and adjacent heat sources and sinks explain Urban Heat Islands in Chicago. *Landscape and Urban Planning* 125, 117–129.
- Dauwalter, D.C., Fesenmyer, K.A., Bjork, R., Leasure, D.R., Wenger, S.J., 2017. Satellite and airborne remote sensing applications for freshwater fisheries. *Fisheries* 42, 526–537.

Demir, B., Bovolo, F., Bruzzone, L., 2012. Updating land-cover maps by classification of image time series: A novel change-detection-driven transfer learning approach. *IEEE Transactions on Geoscience and Remote Sensing* 51, 300–312.

Demir, B., Persello, C., Bruzzone, L., 2011. Batch-Mode Active-Learning Methods for the Interactive Classification of Remote Sensing Images. *IEEE Transactions on Geoscience and Remote Sensing* 49, 1014–1031. <https://doi.org/10.1109/TGRS.2010.2072929>

dos Santos, J.A., Gosselin, P.-H., Philipp-Foliguet, S., Torres, R. da S., Falcão, A.X., 2013. Interactive Multiscale Classification of High-Resolution Remote Sensing Images. *IEEE Journal of Selected Topics in Applied Earth Observations and Remote Sensing* 6, 2020–2034. <https://doi.org/10.1109/JSTARS.2012.2237013>

Espindola, G.M., Câmara, G., Reis, I.A., Bins, L.S., Monteiro, A.M., 2006. Parameter selection for region-growing image segmentation algorithms using spatial autocorrelation. *International Journal of Remote Sensing* 27, 3035–3040.

Falk, T., Mai, D., Besch, R., Çiçek, Ö., Abdulkadir, A., Marrakchi, Y., Böhm, A., Deubner, J., Jäckel, Z., Seiwald, K., 2019. U-Net: deep learning for cell counting, detection, and morphometry. *Nature methods* 16, 67–70.

Ferecatu, M., Boujemaa, N., 2007. Interactive remote-sensing image retrieval using active relevance feedback. *IEEE Transactions on Geoscience and Remote Sensing* 45, 818–826.

Ge, L., Ju, R., Ren, T., Wu, G., 2015. Interactive RGB-D Image Segmentation Using Hierarchical Graph Cut and Geodesic Distance, in: Ho, Y.-S., Sang, J., Ro, Y.M., Kim, J., Wu, F. (Eds.), *Advances in Multimedia Information Processing -- PCM 2015, Lecture Notes in Computer Science*. Springer International Publishing, Cham, pp. 114–124. [https://doi.org/10.1007/978-3-319-24075-6\\_12](https://doi.org/10.1007/978-3-319-24075-6_12)

Gupta, A., Dollar, P., Girshick, R., 2019. Lvis: A Dataset for Large Vocabulary Instance Segmentation, in: *Proceedings of the IEEE/CVF Conference on Computer Vision and Pattern Recognition*. pp. 5356–5364.

Hichri, H., Bazi, Y., Alajlan, N., Malek, S., 2012. Interactive segmentation for change detection in multispectral remote-sensing images. *IEEE Geoscience and Remote Sensing Letters* 10, 298–302.

Hossain, M.D., Chen, D., 2019. Segmentation for Object-Based Image Analysis (OBIA): A review of algorithms and challenges from remote sensing perspective. *ISPRS Journal of Photogrammetry and Remote Sensing* 150, 115–134.

Huang, H., Lan, Y., Yang, A., Zhang, Y., Wen, S., Deng, J., 2020. Deep learning versus Object-based Image Analysis (OBIA) in weed mapping of UAV imagery. *International Journal of Remote Sensing* 41, 3446–3479.

Introduction to the model—ArcGIS pretrained models | Documentation [WWW Document], n.d. URL <https://doc.arcgis.com/en/pretrained-models/latest/imagery/introduction-to-segment-anything-model-sam-.htm> (accessed 1.25.24).

Jang, W.-D., Kim, C.-S., 2019. Interactive Image Segmentation via Backpropagating Refinement Scheme, in: *Proceedings of the IEEE/CVF Conference on Computer Vision and Pattern Recognition*. pp. 5297–5306.

Khanal, S., Fulton, J., Shearer, S., 2017. An overview of current and potential applications of thermal remote sensing in precision agriculture. *Computers and Electronics in Agriculture* 139, 22–32.

Kirillov, A., Mintun, E., Ravi, N., Mao, H., Rolland, C., Gustafson, L., Xiao, T., Whitehead, S., Berg, A.C., Lo, W.-Y., 2023. Segment anything. *arXiv preprint arXiv:2304.02643*.

Kussul, N., Lavreniuk, M., Skakun, S., Shelestov, A., 2017. Deep Learning Classification of Land Cover and Crop Types Using Remote Sensing Data. *IEEE Geoscience and Remote Sensing Letters* 14, 778–782. <https://doi.org/10.1109/LGRS.2017.2681128>

Li, X., Chen, W.Y., Sanesi, G., Laforzezza, R., 2019. Remote sensing in urban forestry: Recent applications and future directions. *Remote Sensing* 11, 1144.

Li, Z., Wang, Y., Zhang, N., Zhang, Y., Zhao, Z., Xu, D., Ben, G., Gao, Y., 2022. Deep Learning-Based Object Detection Techniques for Remote Sensing Images: A Survey. *Remote Sensing* 14, 2385.

Lin, T.-Y., Maire, M., Belongie, S., Hays, J., Perona, P., Ramanan, D., Dollár, P., Zitnick, C.L., 2014. Microsoft Coco: Common Objects in Context, in: European Conference on Computer Vision. Springer, pp. 740–755.

Liu, Q., Xu, Z., Bertasius, G., Niethammer, M., 2022. SimpleClick: Interactive Image Segmentation with Simple Vision Transformers.

Ma, L., Liu, Y., Zhang, X., Ye, Y., Yin, G., Johnson, B.A., 2019. Deep learning in remote sensing applications: A meta-analysis and review. *ISPRS journal of photogrammetry and remote sensing* 152, 166–177.

Moskalenko, A., Shakhuro, V., Vorontsova, A., Konushin, A., Antonov, A., Krapukhin, A., Shepelev, D., Soshin, K., 2024. TETRIS: Towards Exploring the Robustness of Interactive Segmentation [WWW Document]. arXiv.org. URL <https://arxiv.org/abs/2402.06132v1> (accessed 3.3.24).

Nowozin, S., 2014. Optimal decisions from probabilistic models: the intersection-over-union case, in: Proceedings of the IEEE Conference on Computer Vision and Pattern Recognition. pp. 548–555.

Paul, C.K., Mascarenhas, A.C., 1981. Remote sensing in development. *Science* 214, 139–145.

Pavoni, G., Corsini, M., Ponchio, F., Muntoni, A., Edwards, C., Pedersen, N., Sandin, S., Cignoni, P., 2022. TagLab: AI-assisted annotation for the fast and accurate semantic segmentation of coral reef orthoimages. *Journal of Field Robotics* 39, 246–262. <https://doi.org/10.1002/rob.22049>

Portenier, T., Hu, Q., Szabo, A., Bigdeli, S.A., Favaro, P., Zwicker, M., 2018. Faceshop: Deep sketch-based face image editing. arXiv preprint arXiv:1804.08972.

Sofiuk, K., Petrov, I., Barinova, O., Konushin, A., 2020. f-brs: Rethinking backpropagating refinement for interactive segmentation, in: Proceedings of the IEEE/CVF Conference on Computer Vision and Pattern Recognition. pp. 8623–8632.

Sofiuk, K., Petrov, I.A., Konushin, A., 2022. Reviving Iterative Training with Mask Guidance for Interactive Segmentation, in: 2022 IEEE International Conference on Image Processing (ICIP). Presented at the 2022 IEEE International Conference on Image Processing (ICIP), pp. 3141–3145. <https://doi.org/10.1109/ICIP46576.2022.9897365>

Sun, S., Xian, M., Xu, F., Yao, T., Capriotti, L., 2023. CFR-ICL: Cascade-Forward Refinement with Iterative Click Loss for Interactive Image Segmentation. arXiv preprint arXiv:2303.05620.

Suzuki, K., 2017. Overview of deep learning in medical imaging. *Radiological physics and technology* 10, 257–273.

Tewkesbury, A.P., Comber, A.J., Tate, N.J., Lamb, A., Fisher, P.F., 2015. A critical synthesis of remotely sensed optical image change detection techniques. *Remote Sensing of Environment* 160, 1–14.

Uchegbulam, O., Ayolabi, E.A., 2013. Satellite image analysis using remote sensing data in parts of Western Niger Delta, Nigeria. *Journal of Emerging Trends in Engineering and Applied Sciences* 4, 612–617.

Vaihingen 2D Semantic Labeling - ISPRS [WWW Document], n.d. URL <http://www2.isprs.org/commissions/comm2/wg4/vaihingen-2d-semantic-labeling-contest.html> (accessed 6.9.20).

Welcome to the QGIS project! [WWW Document], n.d. URL <https://www.qgis.org/en/site/> (accessed 6.21.23).

Weng, Q., 2012. Remote sensing of impervious surfaces in the urban areas: Requirements, methods, and trends. *Remote Sensing of Environment* 117, 34–49.

Yuan, Q., Shen, H., Li, T., Li, Z., Li, S., Jiang, Y., Xu, H., Tan, W., Yang, Q., Wang, J., 2020. Deep learning in environmental remote sensing: Achievements and challenges. *Remote Sensing of Environment* 241, 111716.

Zhang, S., Liew, J.H., Wei, Y., Wei, S., Zhao, Y., 2020. Interactive object segmentation with inside-outside guidance, in: Proceedings of the IEEE/CVF Conference on Computer Vision and Pattern Recognition. pp. 12234–12244.